Journal of the European Ceramic Society 40 (2020) 5626–5633

Contents lists available at ScienceDirect

Journal of the European Ceramic Society

journal homepage: www.elsevier.com/locate/jeurceramsoc

Original Article

Processing of $Ce_{0.8}Gd_{0.2}O_{2-\delta}$ barrier layers for solid oxide cells: The effect of preparation method and thickness on the interdiffusion and electrochemical performance

S. Molin[a,*], J. Karczewski[b], B. Kamecki[a,b], A. Mroziński[a], S.-F. Wang[c], P. Jasiński[a]

[a] *Advanced Materials Center, Faculty of Electronics, Telecommunications and Informatics, Gdańsk University of Technology, ul. G. Narutowicza 11/12, 80-233 Gdańsk, Poland*
[b] *Advanced Materials Center, Faculty of Applied Physics and Mathematics, Gdańsk University of Technology, ul. G. Narutowicza 11/12, 80-233 Gdańsk, Poland*
[c] *Department of Materials and Mineral Resources Engineering, National Taipei University of Technology, 1, Sec. 3, Chung-Hsiao E. Rd., Taipei 10608, Taiwan, ROC*

ARTICLE INFO

Keywords:
Solid oxide cell
Spray pyrolysis
Ceria
Fuel cell
Electrolysis

ABSTRACT

$Ce_{0.8}Gd_{0.2}O_{1.9}$ (CGO) barrier layers are required to mitigate the chemical reactions between Sr-containing oxygen electrode materials and Zr-based oxygen ion conductors in high-temperature solid oxide cells. Barrier layers produced by different methods were studied in this work. As a reference, a cell with no barrier layer was measured. The application of the powder-processed barrier layers, considerably increases the performance. For further comparison, thin and dense CGO layers were produced by a low-temperature spray pyrolysis process. Three different thicknesses were evaluated: ~300 nm, ~700 nm and ~1500 nm. The best performance was found for the ~700 nm thick CGO barrier layer. It showed low ohmic and polarisation resistances. The low thickness and high density of the CGO barrier layer were found to be the important factors. The cells with the ~700 nm CGO barrier layers were also evaluated for their electrolysis performance as well as fuel cell durability.

1. Introduction

Solid oxide cells (SOCs) are efficient energy conversion devices, which can play an important role in the energy sector. One of the important improvements over the years has been the utilisation of high-performing oxygen electrode materials, i.e. $(La,Sr)(Co,Fe)O_3$ or $(La,Sr)CoO_3$. These mixed ionic-electronic conductors opened the possibility to lower the working temperature of the cells below 800 °C [1,2]. One of the disadvantages of using these materials is their high reactivity with the yttria stabilised zirconia (YSZ) electrolyte, and the formation of poorly conducting $La_2Zr_2O_7$ and $SrZrO_3$ at the electrode-electrolyte interface [3–5]. As a solution to this important problem, an additional diffusion barrier layer between the YSZ and the oxygen electrode can be introduced [6–8]. Doped ceria have found use as the barrier material — it is not reactive with the most popular oxygen electrode materials at typical electrode sintering temperatures (< 1200 °C) [9]. Doped cerias are also good ionic conductors [10–12]. One of the issues when using ceria-based materials is their potential reactivity with YSZ at temperatures exceeding 1200 °C, so sintering at these high temperatures should be avoided. For this reason, different fabrication methods were evaluated, including high temperature powder-based methods [4,13,14] and physical/chemical deposition methods [7,15–17], in which the preparation temperature can be greatly reduced.

High quality CGO barrier layers are crucial for low-temperature high-performance cells. As shown by Zhang-Steenwinkel et al. [18], in a typical porous anode-supported YSZ electrolyte cell, the optimisation of the CGO barrier layer together with a state-of-the-art LSC-based electrode led to the cells having an impressive power density exceeding 1 W cm^{-2} at 600 °C. The dense barrier layer produced via Physical Vapour Deposition (PVD) performed much better than the standard, powder-processed high-temperature co-fired barrier layer. Often, the addition of a CGO barrier layer even a few-nm thick prevents the negative reactions, especially for cells operated at reduced temperatures (< 600 °C) [19,20]. The specific thickness and microstructure that results in the optimised performance of the CGO barrier layers have not yet been rigorously determined.

Spray pyrolysis is a low-temperature ceramic deposition process, used in many areas of materials deposition, including solar cells, catalysis and fuel cells [21–26]. For solid oxide cells, the advantage is that the layers can be prepared at reduced temperature (< 900 °C) [27,28] and the microstructure can be controlled by heat-treatment [29,30].

---

[*] Corresponding author.
E-mail address: sebastian.molin@pg.edu.pl (S. Molin).

https://doi.org/10.1016/j.jeurceramsoc.2020.06.006
Received 29 March 2020; Received in revised form 18 May 2020; Accepted 3 June 2020

The reduction of the fabrication temperature of the CGO barrier layer can be beneficial in lowering the cost of cells, which is an important factor in their broader use. Ceria-based materials have already been produced by spray-pyrolysis, resulting in good performance [5,31–34]. Even though CGO layers produced by spray-pyrolysis were already presented, their long term stability remains an open question.

In this work, we evaluated the electrochemical performance and microstructural features of anode-supported cells with CGO barrier layers with different thicknesses (~300 nm, ~700 nm and ~1500 nm) prepared by spray pyrolysis. In addition, we measured a cell without the barrier layer and with a high-temperature powder-processed CGO coating. In the end, we have also tested the cell for ~500 h and analysed the cell post-mortem. We show the benefit of using dense, readily processed barrier layers on cell performance, caused by lowering of the ohmic resistance, which is substantially higher for the powder processed barrier layers.

2. Experimental

Commercial anode-supported cells were purchased from FuelCellMaterials (ASC2.5 type, USA). They consist of Ni-YSZ/YSZ/GDC/LSC electrodes, optimised to work at < 800 °C. Diameter of a cell was 25 mm, with an oxygen electrode area of 1.23 cm^2. Due to their commercial origin, no preparation details for the CGO barrier layer are available.

Anode-supported half-cells (with no CGO-layers) produced by National Taipei University of Technology (TaipeiTech, Taipei, Taiwan) were used for the deposition of barrier layers. The cells were prepared by tape-casting/screen printing processes. The cells consist of a Ni-YSZ support, Ni-YSZ active electrode and 8 − 10 μm thick YSZ electrolyte. More details about the cells microstructure can be find in [35]. Prior to deposition of the CGO barrier layers, the cells were thoroughly cleaned with acetone and ethanol.

A powder-processed CGO barrier layer was produced by wet-powder spraying of a slurry containing a commercial CGO powder (DC-20 K, DKKK, Japan) in a mixture of toluene and ethanol. A small amount of Co-nitrate (~3 mol.% in respect to CGO) was added to act as a sintering aid. The CoCGO was sprayed on the YSZ electrolyte with a Paasche VLS airbrush. Mass change was measured to control the layer thickness. After deposition, the CoCGO was sintered in air at 1250 °C for 2 h.

Spray pyrolysis processed CGO barrier layers were prepared from liquid solutions containing dissolved Ce- and Gd-nitrates (Sigma-Aldrich, 99.9 % purity). The total concentration of metal cations was 0.2 M. The solution was based on a mixture of tetraethylene glycol and ethanol (99.7 %). Spraying was carried out using a Paasche VLS atomiser. The distance of the nozzle to the substrate was 60 cm, the liquid flow rate was 1 mL/h, and the air pressure set to 2 bar. The hot-plate temperature was 390 °C. The substrates for the deposition were half-cells as well as sapphire (AdValueTech, USA) and YSZ-tape, used for quality control and microstructural evaluation. For the deposition of the ~300 nm, ~700 nm and ~1500 nm thick CGO layers, 5/10/20 mL of the precursor were used. The CGO layers on the half-cells were sintered at 900 °C, and further used for oxygen electrode deposition.

Based on the prepared half-cell, the oxygen electrode was deposited. A commercial $La_{0.6}Sr_{0.4}Co_{0.2}Fe_{0.8}O_{3-\delta}$ (LSCF) paste (Electro-Science Laboratories 4421A, USA) was used. The paste was painted on the samples using a brush, controlling the weight gain (corresponding to the thickness 30 μm). After drying, the LSCF was sintered at 1050 °C for 2 h in air with an intermediate dwell step at 600 °C for 1 h to remove the binder. The sintering temperature was selected based on previous initial measurements of symmetrical cells, for which the best result (the lowest polarisation resistance) was obtained.

The electrochemical characterisation of the cells was based on a custom-built system. The cells (25 mm in diameter) were attached to an alumina tube (25 mm outer diameter, 2 mm wall thickness). The hydrogen electrode was facing the tube. Gold paste was painted on the flat part of the tube edge to electrically connect the hydrogen electrode. The outer edges of the cells were further glued/sealed using a ceramic adhesive (Aremco 552, USA). The oxygen electrode of the cell was painted with Au strips, to which Au wires were attached for electrical contacting. The cell was placed in a tube furnace with PID temperature control. The wires were connected to a Solartron 1260/1287 system for impedance and current-voltage characterisation. After heating to 750 °C (800 °C for the cell with no CGO barrier layer), the reduction of the cell occurred in dry H_2 until a stable OCV value was obtained. The gas inlet line included a small furnace just outside of the main tube furnace, in which a quartz reactor was placed to react O_2 with H_2 to deliver a controlled amount of steam. The temperature of the reactor was maintained at 750 °C, the flows of H_2 and O_2 were controlled by mass flow meters (Brooks, USA). Ambient air was delivered from the other side with a diaphragm pump (500 mL min^{-1}). The system allowed gases to be produced from dry H_2 (as delivered from the hydrogen generator) up to 90 % H_2O – 10 % H_2. To characterise the cells, the impedance spectra were measured at OCV. The impedance data was analysed using the distribution of relaxation times (DRT) method. A freely available DRTTools Matlab script developed by prof. Ciucci was used [36–38]. For cell performance, current-voltage characteristics were measured. The aging of the cell was performed in galvanostatic mode at current densities of 100 mA cm^{-2}, 250 mA cm^{-2} and 500 mA cm^{-2}.

The microstructure of the cells was evaluated using a ThermoFisher Phenom-XL scanning electron microscope (SEM) with an integrated energy dispersive x-ray spectroscopy (EDS) analyser. The SEM imaging was performed at 10 kV acceleration voltage with a backscatter electron (BSE) detector. The EDS analyses were performed using 15 kV acceleration voltage and the ZAF algorithm for quantification. For preparation of polished cross-sections, samples were embedded in epoxy (EpoFix, Denmark), ground and polished down to a 1 μm finish (using a Stuers Tegramin-20 system, Denmark). Before imaging, the epoxy surfaces were sputtered with carbon (Quorum, UK).

The used cell-designations with a short description of the important

Table 1
Specification of tested solid oxide cells.

Cell name:	CGO barrier layer:	CGO thickness:	Notes/remarks:
noCGO	No barrier layer	—	− 2 cells tested;
FCM	Commercial cell with CGO barrier layer	μm, porous	- purchased from FuelCellMaterials, no sintering details available; - $La_{0.6}Sr_{0.4}CoO_{3-\delta}$ (LSC) oxygen electrode; − 2 cells tested;
TT-wpsCGO	Aerosol sprayed CGO barrier layer	3 − 10 μm, porous	- in-house developed cell (TaipeiTech) - cobalt used as a sintering aid, sintered at 1250 °C; − 2 cells tested;
~300 nm	Spray pyrolysis	~300 nm	− 2 cells tested;
~700 nm	Spray pyrolysis,	~700 nm	− 4 cells tested;
~1500 nm	Spray pyrolysis	~1500 nm	− 3 cells tested;

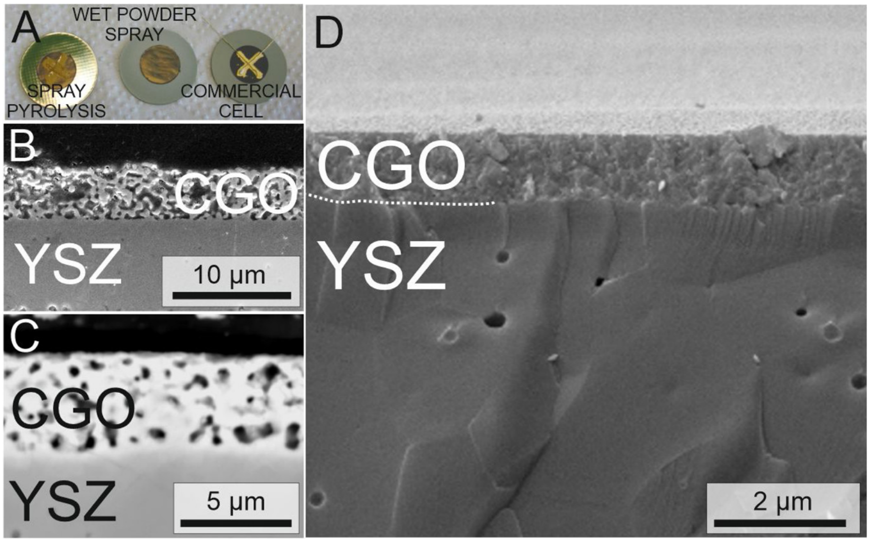

Fig. 1. Microstructure of the CGO layers: A) optical image of the cells with different barrier layers, B) wet-powder spray CGO barrier layer on YSZ electrolyte, C) CGO barrier layer on YSZ electrolyte on a commercial cell (from FuelCellMaterials), D) spray-pyrolysis processed CGO on a YSZ substrate.

features are summarised in Table 1. To ensure reproducibility, several cells of each type were measured. Very good reproducibility was obtained, typically the values (current-voltage, impedance) were within ± 10 %.

3. Results and discussion

3.1. Initial microstructural characterisation

The CGO barrier layers were prepared by spray pyrolysis of liquid precursors and by wet powder spraying of a slurry. For comparison, a commercial state-of-the-art ASC from FuelCellMaterials (USA) was also tested.

Fig. 1 presents images of the different layers produced in this work. The optical picture (Fig. 1 A) shows the different finishes (gloss) of the surfaces. CGO prepared by spray pyrolysis is very glossy. The wet-powder-sprayed CGO layer is the most matte, and the commercial cell has an intermediate appearance.

Fig. 1 B shows the polished cross section of the wet-powder-sprayed CGO coating on the YSZ electrolyte. It was deposited on an already pre-sintered NiO-YSZ/YSZ half-cell. Due to constrained sintering, the layer cannot shrink and densify. The layer is thus porous (40–50 % porosity) and ~5 µm thick. Fig. 1 C presents a cross-section of the commercial cell with the CGO on top of the dense YSZ layer. The CGO coating is denser than the one shown in Fig. 1 B. The preparation details are not known. These two powder-processed CGO coatings resemble the typical powder-processed barrier layers reported in the literature. These coatings are used as the reference ones in this work.

Fig. 1 D shows the fracture cross-section microstructure of the CGO layer produced by spray-pyrolysis on a ~150 µm thick YSZ substrate. The layer structure seems dense and has a thickness of ~1 µm. The fracture cross section image shows good adherence and density of the layer. As presented in the images, the microstructures of CGO prepared by wet powder spray and spray pyrolysis are thus vastly different. Even though the spray-pyrolysis produced CGO has been sintered at 900 °C, it has a visibly denser microstructure than the powder processed CGO layers produced at > 1200 °C.

3.2. Electrochemical and post-mortem analysis

The influence of the different barrier layers on cell performance has been assessed through electrochemical characterisation. For reference, cells without barrier layers were also measured. The results are presented in Supplementary materials (Figure S1). As expected, the lack of a barrier layer results in very high polarisation resistance. The ohmic resistance of the cell without the CGO barrier layer has been unexpectedly low, but it might be partly due to higher testing temperature (800 °C).

3.3. Powder-processed CGO barrier layers

In this part, we evaluate two types of cells with powder-processed CGO barrier layers. The first type is a commercially available hydrogen electrode supported cell with a CGO barrier layer and an LSC oxygen electrode (FCM cell). The second type is a hydrogen electrode supported cell produced by TaipeiTech with CGO produced in-house via wet powder spray and with an LSCF oxygen electrode (TT-wpsCGO cell).

The electrochemical performance of the cells is presented in Fig. 2 A. The two cells show very similar performance. The maximum power density reaches ~800 mW cm^{-2}, two orders of magnitude higher than in the case of the cells with no barrier layer (which were tested at 800 °C), presented in Figure S1. The current-voltage measurements are supplemented by impedance measurements, carried out at OCV. The spectra are presented in Fig. 2 B. The ohmic resistance of the TT-wpsCGO cell is lower than the ohmic resistance of the commercial FCM cell. Generally, the values of $0.15-0.20\ \Omega\ cm^2$ are obtained at 750 °C. Recalculated for the electrolyte thickness of 10 µm (including both the CGO and YSZ), the resulting specific conductivity value is ~$5-10$ mS cm^{-1}, which is slightly below the conductivity of pure YSZ (~20 mS cm^{-1}) and CGO (~60 mS cm^{-1}). The ohmic resistance also includes, however, contributions from the non-ideal contacts, the porosity of both electrolytes, etc. Adversely, the polarisation resistance of the TT-wpsCGO cell is higher. The sum of the ohmic and polarisation resistances is the same for the two cells, resulting in the same performance. Based on the DRT analysis (the inset of Fig. 2 B), the individual processes on both cells differ: the high (P1~1000 Hz) and medium (P2~20 Hz) frequency process alters their relative intensities. The low frequency process (P3~0.1 Hz) remains similar for the two cells.

Based on the available literature, the process between 1000–10,000 Hz can possibly be ascribed to the Ni/YSZ triple phase boundary, while the processes at 100–1000 Hz to the oxygen electrode. The process at 100–10 Hz can be related to gas diffusion, while the processes at frequencies < 10 Hz to gas conversion [39–41]. For a relatively small cell size, gas conversion has a small effect [42]. This is however only a generalised, simplistic view of the complex electrodes in a full fuel cell.

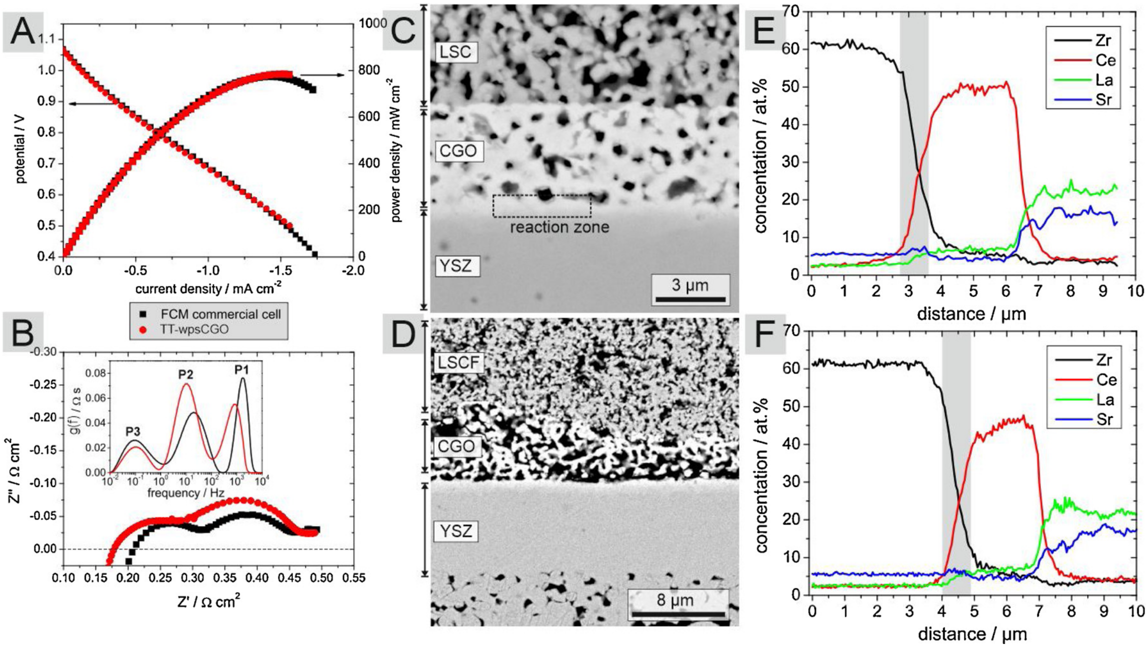

Fig. 2. Electrochemical performance of the cells with powder processed CGO layers: A) current-voltage and power density characteristics, B) impedance spectroscopy, C and D) SEM cross-section analysis of FCM commercial and TT-wpsCGO cell, respectively, E and F) EDS elemental line scan analyses of FCM commercial and TT-wpsCGO cell, respectively.

An equivalent circuit consisting of as many as six frequency-dependent processes is used to determine cell spectra in the literature [40,42].

In the DRT spectra presented in the inset in Fig. 2 B, the predicted contribution from the oxygen electrode (characteristic frequency between 100–1000 Hz) is not distinguishable. One reason is that it has a very small magnitude. Indeed, based on CGO-based symmetrical electrode measurements of the porous LSCF electrode, low polarisation resistances ($<$ 20 mΩ cm^2) at 750 °C can be achieved [43]. Though the measurements from the symmetrical cells are not directly applicable for fuel cell performance determination, they indicate very high performance of the LSCF electrode. The contribution of the oxygen electrode to the total polarisation of the fuel cell can be thus summarised as very small [44].

The microstructures of the commercial and in-house developed cells are presented in Fig. 2 C–D. The commercial cell has a ~5 µm thick CGO layer with porosity ~30 %. The in-house developed cell shows a more porous and slightly thicker CGO layer. Line-scans across the CGO/YSZ interfaces are shown in Fig. 2 E–F. There is only a very small, but nonetheless noticeable increase of the Sr signal at the CGO/YSZ interface. As has been reported, it most probably comes from the sintering step, where the layers are exposed to high temperatures. Kiebach et al. has shown that a $SrZrO_3$ layer forms upon sintering of a LSCF/CGO electrode (sintered at 1250 °C), and does not progress further during a 1600 h cell test at 0.5 A cm^{-2} [4].

The application of a porous CGO barrier layer, achievable by relatively simple powder-processing routes, results in a two-fold order of magnitude increase in power density in comparison to a cell without the barrier layer. Even though the layer can be quite porous, it is still effective at blocking the formation of the $SrZrO_3$ phase.

3.4. CGO barrier layers produced by spray-pyrolysis

Spray-pyrolysis was used to deposit CGO barrier layers and compare their properties with the powder-processed ones. The main advantage of the spray-pyrolysis process is that it is possible to fabricate ceramic layers at reduced temperatures, e.g. at ~400 °C. For screening purposes, samples with three different thicknesses of the barrier layer were produced. Different thicknesses were achieved by spraying different amounts of the precursor-solution onto the samples. Cells with thicknesses of ~300 nm, ~700 nm, and ~1500 nm were produced and studied. The thicknesses used for the description of the samples are average CGO thicknesses, as determined from several SEM images. Generally, the thickness has some variation (max ± 20 %) caused mainly by the surface irregularities. On very flat surfaces (e.g. single crystals), spray-pyrolysis produces very flat and uniform layers. On surfaces with some irregularities, deposits tend to be thicker at convex surfaces (in the "valleys"). As the YSZ electrolyte has some irregularities in thickness (in the range of ± 10 %), it is also visible in the CGO thickness variability.

The effect of the CGO thickness on the electrochemical performance is presented in Fig. 3 A. The lowest performance among the cells is shown, expectedly, by the cell with the ~300 nm thick CGO, which has a maximum power density of ~700 mW cm^{-2}. The best performance is achieved by the cell with the ~700 nm thick ceria layer. In this case, the maximum power density reaches ~1 W cm^{-2}. For the cell with the thickest CGO barrier layer (~1500 nm), an intermediate value of the power density is achieved. The results were confirmed based on measurements of several cells. Specifically, the ~1500 nm CGO barrier layer resulted in lowered performance.

The results of the impedance analysis of the three cells, measured at OCV, are presented in Fig. 3 B. The cell with the thinnest CGO layer shows the highest ohmic resistance (~0.14 Ω cm^2) and the largest polarisation resistance (~0.15 Ω cm^2). The two cells with thicker CGO layers have a quite low series resistance (90–100 mΩ cm^2), which would correspond to the specific conductivity of ~11 mS cm^{-1}. Slightly lower ohmic resistance has been obtained for the 700 nm cells, which resulted in higher performance under a current load. This is a visible improvement over the samples with the powder-processed CGO barrier layer. As evidenced in Fig. 1, the spray-pyrolysis produced layers have a dense microstructure and are quite thin. Both of these features contribute towards the lower ohmic resistance.

The polarisation resistance of the cells with ~700 nm and ~1500 nm thick CGO barrier layers is quite similar, i.e. 0.12 Ω cm^2 at OCV. The electrode performance at OCV is thus the same for both cells. The resulting performance is better for the cell with the ~700 nm CGO layer. The comparison of the individual contributions to the spectra

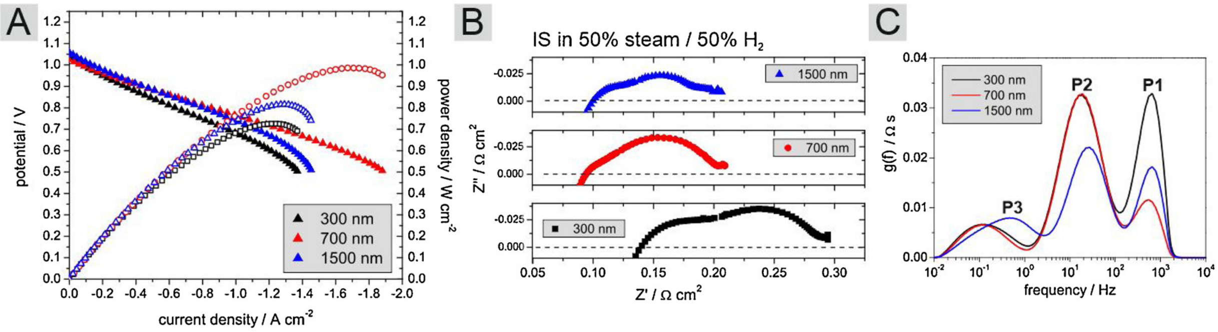

Fig. 3. Electrochemical performance of CGO barrier layers prepared by spray pyrolysis: A) current-voltage and power density characteristics, B) impedance spectra of cells, C) DRT analysis of spectra shown in B).

presented in Fig. 3 B shows different behaviour, especially for the low frequency process.

The overall resistance of the cells (measured in 50 % steam/50 % H_2 at OCV), including the series and polarisation contributions, is ~0.2 Ωcm^2 for the cells with the ~700 nm, and ~1500 nm thick CGO, and ~0.3 Ω cm^2 for the cell with the ~300 nm CGO.

Even though the performance of the cells with 700 nm and 1500 nm CGO layers is quite similar at OCV, they differ under the current load. The cell with ~1500 nm CGO layer shows larger activation polarisation than the cell with ~700 nm thick CGO, which results in different performance at higher current densities. To take that into account, in addition to performance parameters determined by impedance spectroscopy at OCV, ASR has been also calculated based on the current-voltage plot (Fig. 3 A). The slope of the curves has been determined in the voltage range 800 mV – 700 mV and is included in Table 2 as the "Tangent ASR" values.

The parameters of the cells based on the impedance and current-voltage measurements are summarised in Table 2.

The higher performance of the cells with 700 nm thick CGO layers in comparison to the cells with 1500 nm thick CGO layer is noteworthy. The tangent ASR values obtained for these two cells are considerably different. We hypothesize, that one of the possible reasons can be a large number of (resistive) grain boundaries in the spray-pyrolysis produced layers, resulting in their low total conductivity [32] (but in general still better than for the thick and highly porous powder processed layers). So the positive effect of the barrier layer is visible when the negative interdiffusion is blocked, but a further increase of the barrier layer thickness does not result in performance improvements.

The microstructures and respective elemental line-scans of the three cells are presented in Fig. 4. Even though the resolution of EDS is typically within ± 0.5 μm, it can be used to qualitatively analyse the reactivity of the fabricated barrier layers, as also confirmed in the literature [4]. The different thicknesses of the CGO barrier layers are confirmed in the EDS line-scans as broader and more intense profiles of Ce. For the cell with a ~300 nm CGO, a sort of delamination/disintegration of the CGO can be noticed. A small part of the barrier layer separated at the bottom almost as a continuous layer. It is probably caused by some reaction between the YSZ and Sr-containing oxygen electrode. The Sr signal extends further than the La signal in the line-scan, confirming the reaction. In the case of the ~700 nm thick CGO, the ceria separates the YSZ from the LSCF more clearly, which is even more clear for the thicker layer. For the ~700 nm CGO layer, the Sr profile also extends into the barrier layer. For the two thicker CGO barrier layers (~300 nm and ~700 nm), no signs of reaction were detected (seen as possible discolouration in the SEM images).

Based on the results presented in Figs. 2,3,4, and the data summarised in Table 2, we conclude that the improvement in cell performance comes from the decreased ohmic resistance of the cell, achieved by application of a relatively thin and dense CGO barrier layer by spray pyrolysis.

3.5. Durability of the cells with the implemented barrier layer

Based on the analyses presented above, the cell with the ~700 nm thick CGO was selected for further studies. The current-voltage characteristics of the cell in electrolysis cell (EC) and fuel cell (FC) modes are presented in Fig. 5. The characterisation was performed in gases containing different amounts of steam and hydrogen, from dry H_2 to 90 vol.% $H_2O + 10$ % H_2.

The cell shows reversible behaviour (no change of slope when switching between FC/EC modes), showing high performance in electrolysis mode. In an atmosphere containing 50 % steam with 50 % H_2, the current obtained at thermoneutral voltage is -1.25 A cm^{-2}. In a higher steam content atmosphere with 90 % steam, the current at V_{tn} exceeds -1.75 A cm^{-2}. For cells operating at 750 °C, these are very good results. For comparison, a state-of-the-art cell with an infiltrated hydrogen electrode has shown a current density of -1 A at 1.15 V in 90/10 H_2O/H_2 at 800 °C (70 % steam conversion), whereas our cells show a slightly higher performance even at 750 °C (but at much lower conversion, < 10 %). The fuel cell performance is also good; a maximum power density of ~1 W cm^{-2} can be achieved. The cell loses power only slightly when operated in 50:50 steam:H_2 gas in comparison to pure hydrogen.

The impedance spectra measured at OCV as a function of the steam content are presented in Fig. 5 C, and the respective DRT plots are presented in Fig. 5 D. The pH_2O has an effect on the higher frequency and lower frequency processes, which might indicate that these processes are related to the hydrogen electrode (as the gas on the oxygen

Table 2
Parameters of the cells with different barrier layers.

Cell name:	Description	Ohmic resistance: mΩ cm^2	Polarisation resistance: mΩ cm^2	Total ASR at OCV: mΩ cm^2	Tangent ASR: mΩ cm^2	Maximum power density: mW cm^{-2}
Cell-0	No barrier layer (800 °C)	82	17,300	17,382	~39,100	8
Cell-1	Commercial cell	184	305	489	325	800
Cell-2	Powder-processed CGO	173	136	309	325	800
Cell-3	~300 nm CGO	140	154	294	324	730
Cell-4	~700 nm CGO	95	114	209	235	990
Cell-5	~1500 nm CGO	100	106	206	306	810

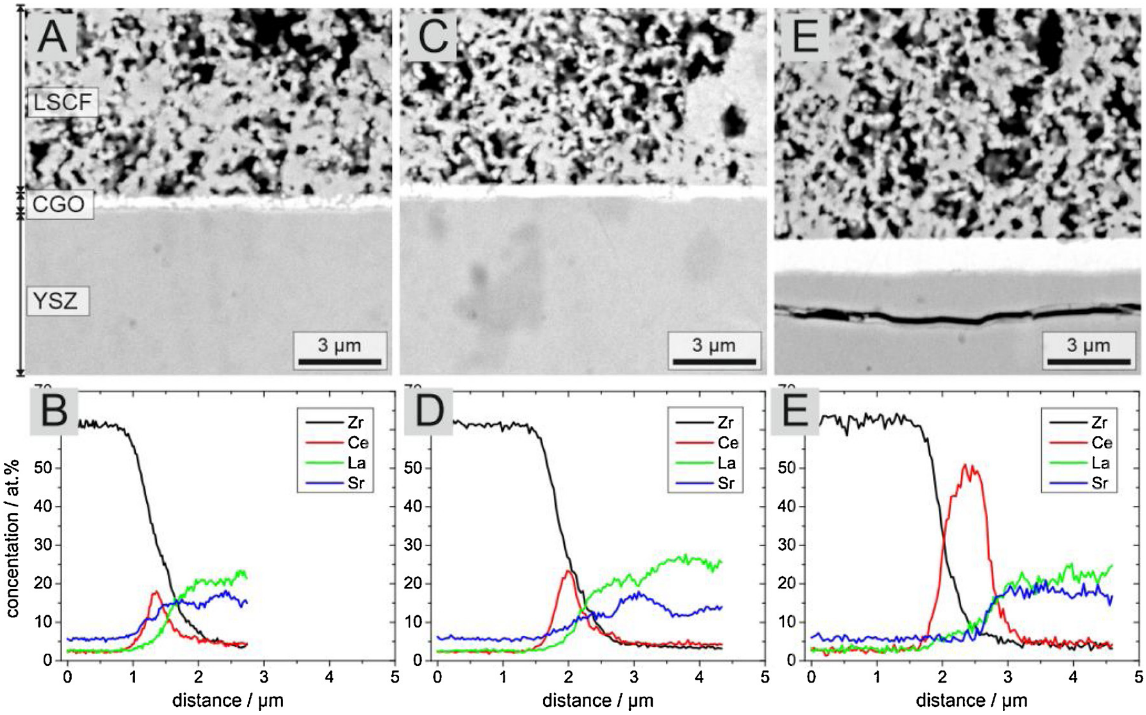

Fig. 4. Microstructure and elemental line-scans of the cells with CGO prepared by spray pyrolysis: A and B) with 300 nm CGO; C and D) with ∼700 nm CGO; E and F) with ∼1500 nm CGO.

side was not changed). P1 has been ascribed to the Ni/YSZ-tpb reaction, whereas the P2 and P3 can be possibly ascribed to gas conversion. Interestingly, P1 intensity decreases monotonically with the pH_2O increase. For P2 and P3, the increase of pH_2O from 0% to 50 % also results in decreasing intensity of the peaks, which increases again for a steam rich atmosphere.

The cell was tested for durability in fuel cell working mode. After the initial testing, the cell was operated at current densities of 100 mA cm^{-2}, 250 mA cm^{-2}, and 500 mA cm^{-2} for 10 h, 90 h, and ∼420 h, reaching ∼520 h in total. The voltage development of the cell during operation is presented in Fig. 6 A. The initial power density reached a value of ∼1050 mW cm^{-2} after some initial increase in the first few hours. After ∼520 h, the power density is lowered to ∼600 mW cm^{-2} as shown in Fig. 6 B. The cell degraded quite considerably during the

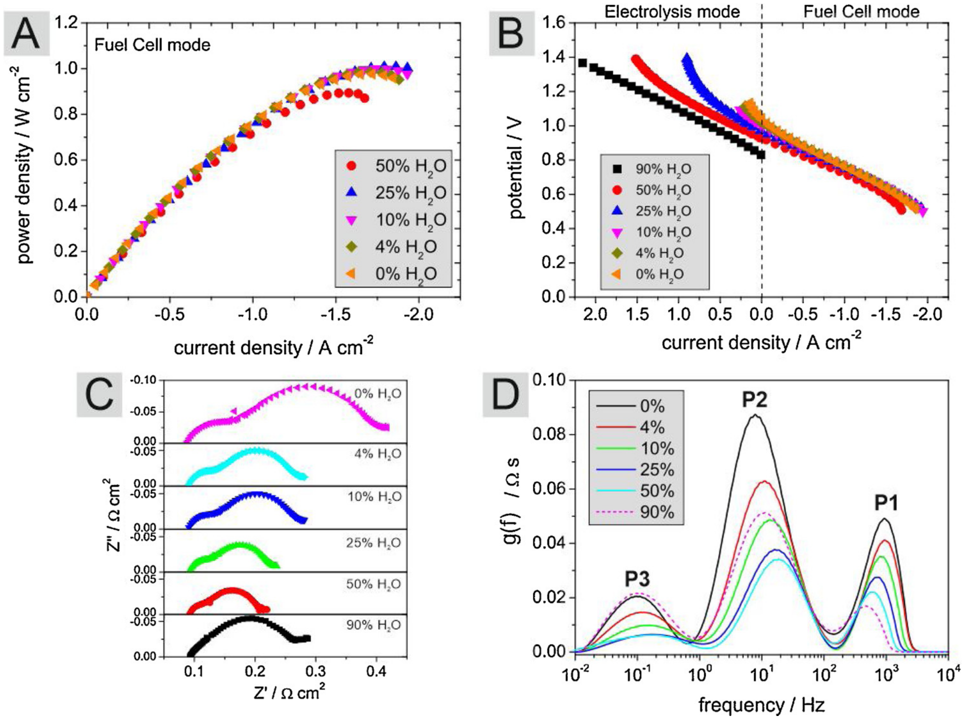

Fig. 5. Electrochemical performance of cell with ∼700 nm CGO layer prepared by spray pyrolysis: A) power density characteristics, B) current-voltage characteristics, C) impedance spectra, D) DRT analysis of spectra shown in C).

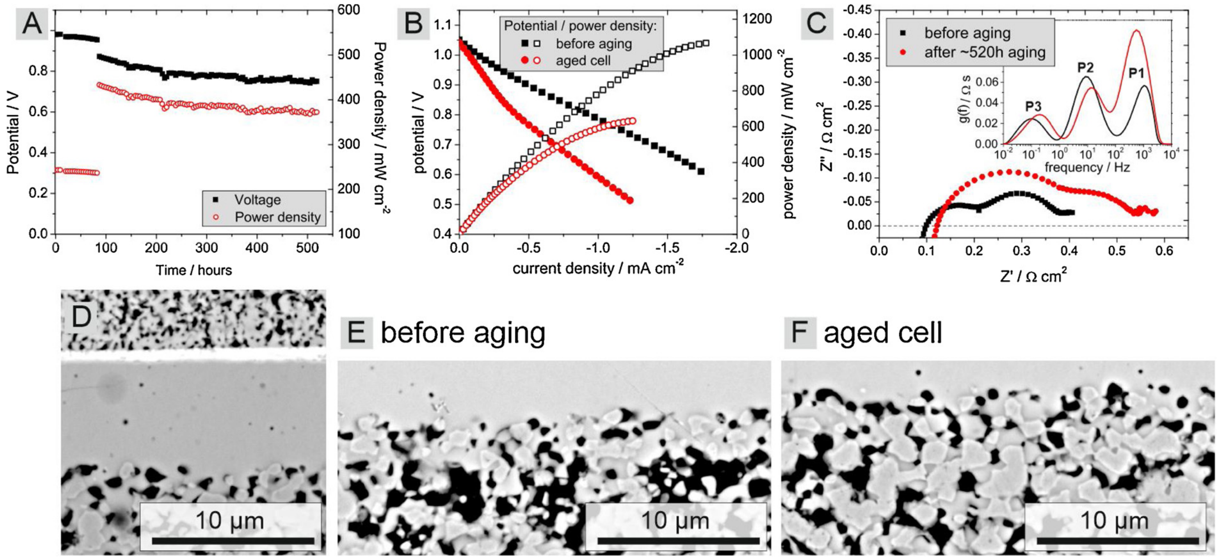

Fig. 6. Results of longer term performance test: A) cell potential / power density vs. time and current load, B) current voltage and power density characteristics, C) impedance spectra and DRT analysis, D) microstructure of the aged cell and hydrogen electrode active regions: E) before and F) after aging.

first 300 h, but then the degradation rate lowered and flattened for the last ~100 h. Comparing the impedance plots shown in Fig. 6 C, changes in the ohmic resistance and electrode polarisation can be seen. The ohmic resistance increases from ~100 mΩ cm^2 to 122 mΩ cm^2, which constitutes a 30 % relative increase. The inset of Fig. 6 C shows DRT plots of the impedance spectra. As seen in the spectra, a large increase of the higher frequency electrode polarisation process (P1) occurred. The resistance of this process almost tripled. The lower frequency contributions (P2 and P3) have very similar values before and after aging.

The P1 process, being connected to Ni/YSZ-tpb, drives the degradation of the fuel cell. The degradation is caused by nickel segregation, coarsening etc, and is a typical degradation process observed for nickel-YSZ electrodes [44,45].

Microstructural analysis of the cell after aging confirmed changes in hydrogen electrode microstructure and no visible change in the CGO barrier layer microstructure (Fig. 6 D and Figure S2). Comparing the electrochemically active region of the hydrogen electrode (close to the interface with the YSZ electrolyte) between the cell before aging (Fig. 6E) and after aging (Fig. 6F), nickel agglomeration can be observed. In the initial state, some nickel particles could be found directly at the interface with YSZ, but after aging, the number of these particles seems to be visibly lower.

4. Conclusions

In this work, several types of CGO barrier layers were evaluated for their effectiveness in blocking the interdiffusion between an Sr-containing oxygen electrode and a YSZ electrolyte. A cell with no barrier layer showed high electrode polarisation resulting in very low power density. Powder-processed CGO layers, with thicknesses in the range 5 − 10 µm, on both a commercial and in-house developed cell showed good performance, however they show a small diffusion of Sr to the YSZ, which probably occurred during the high temperature sintering of the layers (> 1000 °C). Alternative, low-temperature processed barrier layers were produced by the spray-pyrolysis process. These layers showed high efficiency in blocking the interdiffusion. The thinnest evaluated barrier layer, ~300 nm thick, resulted in performance only slightly inferior to the powder processed layers. The thicker layers, with thicknesses of ~700 nm and 1500 nm, resulted in improved performance. The overall best performance was found for the ~700 nm thick CGO barrier layer. It showed low ohmic resistance, low electrode polarisation and resulted in a power density ~1 W cm^{-2} at 750 °C. Based on the results, the main advantage of using spray-pyrolysis barrier layers is their low ohmic resistance, resulting directly in increased cell performance. Detailed studies of the in-house developed cell (at TaipeiTech) with the ~700 nm CGO barrier layer were performed, including tests in fuel cell and electrolysis modes. The cell showed high current densities in electrolysis mode. At a thermoneutral voltage of 1.29 V, the current density exceeded 1.7 A cm^{-2} at 750 °C (in 90 % H_2O + 10 % H_2). The durability of the cell was studied in fuel cell mode. The 500 -h-long test showed degradation, decreasing the power output from the initial 1000 mW cm^{-2} to ~600 mW cm^{-2}. This is likely caused by Ni/YSZ-tpb degradation, not directly related to the barrier layers. Therefore, the spray-pyrolysis developed barrier layers are very promising candidates for high performance cells, offering performances higher than those achieved for typical, powder-processed barrier layers.

Declaration of Competing Interest

The authors declare that they have no known competing financial interests or personal relationships that could have appeared to influence the work reported in this paper

Acknowledgements

This project was supported by the project funded by National Science Centre Poland based on decision2017/25/B/ST8/02275 “Understanding and minimization of ohmic and polarization losses in solid oxide cells by nanocrystalline ceramic and cermet functional layers” and by the ministry research subsidy for the Gdańsk University of Technology.

Appendix A. Supplementary data

Supplementary material related to this article can be found, in the online version, at doi:https://doi.org/10.1016/j.jeurceramsoc.2020.06.006.

References

[1] I. Garbayo, F. Baiutti, A. Morata, A. Tarancón, Engineering mass transport properties in oxide ionic and mixed ionic-electronic thin film ceramic conductors for energy applications, J. Eur. Ceram. Soc. 39 (2019) 101–114, https://doi.org/10.

1016/j.jeurceramsoc.2018.09.004.

[2] D. Roehrens, F. Han, M. Haydn, W. Schafbauer, D. Sebold, N.H. Menzler, H.P. Buchkremer, Advances beyond traditional SOFC cell designs, Int. J. Hydrogen Energy 40 (2015) 11538–11542, https://doi.org/10.1016/j.ijhydene.2015.01.155.

[3] K. Cheng, H. Xu, L. Zhang, Y. Du, J. Zhou, S. Tang, M. Chen, Numerical simulation of the SrZrO 3 formation in solid oxide fuel cells, J. Korean Inst. Electr. Electron. Mater. Eng. (2019), https://doi.org/10.1007/s11664-019-07236-0.

[4] R. Kiebach, W.-W. Zhang, W. Zhang, M. Chen, K. Norrman, H.-J. Wang, J.R. Bowen, R. Barfod, P.V. Hendriksen, Stability of La0.6Sr0.4Co0.2Fe0.8O3/Ce0.9Gd0.1O2 cathodes during sintering and solid oxide fuel cell operation, J. Power Sources 283 (2015) 151–161, https://doi.org/10.1016/j.jpowsour.2015.02.064.

[5] L. dos Santos-Gómez, J. Hurtado, J.M. Porras-Vázquez, E.R. Losilla, D. Marrero-López, Durability and performance of CGO barriers and LSCF cathode deposited by spray-pyrolysis, J. Eur. Ceram. Soc. 38 (2018) 3518–3526, https://doi.org/10.1016/j.jeurceramsoc.2018.03.024.

[6] P. Plonczak, M. Joost, J. Hjelm, M. Sogaard, M. Lundberg, P.V. Hendriksen, A high performance ceria based interdiffusion barrier layer prepared by spin-coating, J. Power Sources 196 (2011) 1156–1162, https://doi.org/10.1016/j.jpowsour.2010.08.108.

[7] S. Sønderby, T. Klemensø, B.H. Christensen, K.P. Almtoft, J. Lu, L.P. Nielsen, P. Eklund, Magnetron sputtered gadolinia-doped Ceria diffusion barriers for metal-supported solid oxide fuel cells, J. Power Sources 267 (2014) 452–458, https://doi.org/10.1016/j.jpowsour.2014.05.101.

[8] S. Ovtar, M. Chen, A.J. Samson, R. Kiebach, In-situ formed Ce0.8Gd0.2O1.9Barrier layers on yttria stabilized zirconia backbones by infiltration - A promising path to high performing oxygen electrodes of solid oxide cells, Solid State Ion. 304 (2017) 51–59, https://doi.org/10.1016/j.ssi.2017.03.019.

[9] H. Xu, K. Cheng, M. Chen, L. Zhang, K. Brodersen, Y. Du, Interdiffusion between gadolinia doped ceria and yttria stabilized zirconia in solid oxide fuel cells: experimental investigation and kinetic modeling, J. Power Sources 441 (2019) 227152, https://doi.org/10.1016/j.jpowsour.2019.227152.

[10] M. Mogensen, N.M. Sammes, G.A. Tompsett, Physical, chemical and electrochemical properties of pure and doped ceria, Solid State Ion. 129 (2000) 63–94, https://doi.org/10.1016/S0167-2738(99)00318-5.

[11] C. Chatzichristodoulou, P.T. Blennow, M. Søgaard, P.V. Hendriksen, M.B. Mogensen, Ceria and Its Use in Solid Oxide Cells and Oxygen Membranes, 2nd editio, Catal. by Ceria Relat. Mater, 2013, pp. 623–782.

[12] S. Cheng, C. Chatzichristodoulou, M. Søgaard, A. Kaiser, P.V. Hendriksen, Ionic/Electronic Conductivity, Thermal/Chemical Expansion and Oxygen Permeation in Pr and Gd Co-Doped Ceria $Pr_x Gd_{0.1} Ce_{0.9-x} O_{1.95-\delta}$, J. Electrochem. Soc. 164 (2017) F1354–F1367, https://doi.org/10.1149/2.0531713jes.

[13] D.W. Ni, V. Esposito, S.P.V. Foghmoes, S. Ramousse, Densification and grain growth kinetics of Ce0.9Gd0.1O1.95 in tape cast layers: the influence of porosity, J. Eur. Ceram. Soc. 34 (2014) 2371–2379, https://doi.org/10.1016/j.jeurceramsoc.2014.02.039.

[14] X. Dan, C. Wang, X. Xu, Y. Liu, X. Cheng, M. Fronzi, L. Bi, X.S. Zhao, Improving the sinterability of CeO2 by using plane-selective nanocubes, J. Eur. Ceram. Soc. 39 (2019) 4429–4434, https://doi.org/10.1016/j.jeurceramsoc.2019.06.024.

[15] S. Uhlenbruck, N. Jordan, D. Sebold, H.P. Buchkremer, V.A.C. Haanappel, D. Stöver, Thin film coating technologies of (Ce,Gd)O2-δ interlayers for application in ceramic high-temperature fuel cells, Thin Solid Films 515 (2007) 4053–4060, https://doi.org/10.1016/j.tsf.2006.10.127.

[16] D. Szymczewska, A. Chrzan, J. Karczewski, S. Molin, P. Jasinski, Spray pyrolysis of doped-ceria barrier layers for solid oxide fuel cells, Surf. Coatings Technol. 313 (2017) 168–176, https://doi.org/10.1016/j.surfcoat.2017.01.066.

[17] C. Sındıraç, H. Büyükaksoy, S. Akkurt, Electrical properties of gadolinia doped ceria electrolytes fabricated by infiltration aided sintering, Solid State Ion. 340 (2019), https://doi.org/10.1016/j.ssi.2019.115020.

[18] Y. Zhang-Steenwinkel, Q. Yu, F.P.F. van Berkel, M.M.A. van Tuel, B. Rietveld, H. Tu, High performance solid-oxide fuel cell: opening windows to low temperature application, Int. J. Hydrogen Energy 41 (2016) 5824–5832, https://doi.org/10.1016/j.ijhydene.2016.02.033.

[19] W. Jung, H.L. Tuller, Investigation of Cathode Behavior of Model Thin-Film SrTi [sub 1 − x]Fe[sub x]O[sub 3 − δ] ($x = 0.35$ and 0.5) Mixed Ionic-Electronic Conducting Electrodes, J. Electrochem. Soc. 155 (2008) B1194, https://doi.org/10.1149/1.2976212.

[20] W. Jung, H.L. Tuller, Impedance study of SrTi(1-x)Fe(x)O(3-delta) ($x = 0.05$ to 0.80) mixed ionic-electronic conducting model cathode, Solid State Ion. 180 (2009) 843–847, https://doi.org/10.1016/j.ssi.2009.02.008.

[21] C.-Y. Chen, K.-H. Chang, H.-Y. Chiang, S.-J. Shih, Preparation of a porous Ceria coating for a resistive oxygen sensor, Sensors Actuators B Chem. 204 (2014) 31–41, https://doi.org/10.1016/j.snb.2014.07.053.

[22] Y. Zhang, R. Knibbe, J. Sunarso, Y. Zhong, W. Zhou, Z. Shao, Z. Zhu, Recent progress on advanced materials for solid-oxide fuel cells operating below 500 °C, Adv. Mater. 1700132 (2017) 1700132, https://doi.org/10.1002/adma.201700132.

[23] D. Perednis, L.J. Gauckler, Thin film deposition using spray pyrolysis, J. Electroceramics. 14 (2005) 103–111, https://doi.org/10.1007/s10832-005-0870-x.

[24] C. Guild, S. Biswas, Y. Meng, T. Jafari, A.M. Gaffney, S.L. Suib, Perspectives of spray pyrolysis for facile synthesis of catalysts and thin films: an introduction and summary of recent directions, Catal. Today 238 (2014) 87–94, https://doi.org/10.1016/j.cattod.2014.03.056.

[25] M.J. Escudero, M.P. Yeste, M.Á. Cauqui, M.A. Munoz, Performance of direct methane solid oxide fuel cell using nickel-ceria-Yttria stabilized zirconia as the anode, Materials Basel (Basel) 13 (2020).

[26] L. Santos-gómez, J.M. Porras-vázquez, E.R. Losilla, F. Martín, J.R. Ramos-barrado, LSCF-CGO nanocomposite cathodes deposited in a single step by spray- pyrolysis, J. Eur. Ceram. Soc. 38 (2018) 1647–1653, https://doi.org/10.1016/j.jeurceramsoc.2017.10.010.

[27] B. Kamecki, J. Karczewski, H. Abdoli, M. Chen, G. Jasiński, P. Jasiński, S. Molin, Deposition and electrical and structural properties of La0.6Sr0.4CoO3 thin films for application in high-temperature electrochemical cells, J. Korean Inst. Electr. Electron. Mater. Eng. 48 (2019) 5428–5441, https://doi.org/10.1007/s11664-019-07372-7.

[28] B. Kamecki, J. Karczewski, T. Miruszewski, G. Jasiński, D. Szymczewska, P. Jasiński, S. Molin, Low temperature deposition of dense MnCo2O4protective coatings for steel interconnects of solid oxide cells, J. Eur. Ceram. Soc. 38 (2018) 4576–4579, https://doi.org/10.1016/j.jeurceramsoc.2018.05.042.

[29] B. Scherrer, J. Martynczuk, H. Galinski, J.G. Grolig, S. Binder, A. Bieberle-Hütter, J.L.M. Rupp, M. Prestat, L.J. Gauckler, Microstructures of YSZ and CGO thin films deposited by spray pyrolysis: influence of processing parameters on the porosity, Adv. Funct. Mater. 22 (2012) 3509–3518, https://doi.org/10.1002/adfm.201200454.

[30] J.L.M. Rupp, B. Scherrer, A.S. Harvey, L.J. Gauckler, Crystallization and grain growth kinetics for precipitation-based ceramics: a case study on amorphous ceria thin films from spray pyrolysis, Adv. Funct. Mater. 19 (2009) 2790–2799, https://doi.org/10.1002/adfm.200900255.

[31] G. Nurk, M. Vestli, P. Mo ller, R. Jaaniso, M. Kodu, H. Ma ndar, T. Romann, R. Kanarbik, E. Lust, Mobility of Sr in gadolinia doped Ceria barrier layers prepared using spray pyrolysis, pulsed laser deposition and magnetron sputtering methods, J. Electrochem. Soc. 163 (2015) F88–F96, https://doi.org/10.1149/2.0531602jes.

[32] B. Kamecki, J. Karczewski, P. Jasiński, S. Molin, Evaluation of praseodymium and gadolinium doped ceria as a possible barrier layer material for solid oxide cells, ECS Trans. (2019), https://doi.org/10.1149/09101.1165ecst.

[33] D. Szymczewska, J. Karczewski, A. Chrzan, P. Jasinski, CGO as a barrier layer between LSCF electrodes and YSZ electrolyte fabricated by spray pyrolysis for solid oxide fuel cells, Solid State Ion. 302 (2017) 113–117, https://doi.org/10.1016/j.ssi.2016.11.008.

[34] L. dos Santos-Gómez, J. Zamudio-García, J.M. Porras-Vázquez, E.R. Losilla, D. Marrero-López, Highly oriented and fully dense CGO films prepared by spray-pyrolysis and different precursor salts, J. Eur. Ceram. Soc. 40 (2020) 3080–3088, https://doi.org/10.1016/j.jeurceramsoc.2020.03.026.

[35] B. Hołówko, J. Karczewski, S. Molin, P. Jasiński, Preparation of Hydrogen Electrodes of Solid Oxide Cells by Infiltration: Effects of the Preparation Procedure on the Resulting Microstructure, Materials Basel (Basel) 13 (2019) 131, https://doi.org/10.3390/ma13010131.

[36] M. Saccoccio, T.H. Wan, C. Chen, F. Ciucci, Optimal regularization in distribution of relaxation times applied to electrochemical impedance spectroscopy: ridge and Lasso regression methods - A theoretical and experimental Study, Electrochim. Acta 147 (2014) 470–482, https://doi.org/10.1016/j.electacta.2014.09.058.

[37] F. Ciucci, C. Chen, Analysis of electrochemical impedance spectroscopy data using the distribution of relaxation times: a bayesian and hierarchical bayesian approach, Electrochim. Acta 167 (2015) 439–454, https://doi.org/10.1016/j.electacta.2015.03.123.

[38] E. Quattrocchi, T.H. Wan, A. Curcio, S. Pepe, M.B. Effat, F. Ciucci, A general model for the impedance of batteries and supercapacitors: The non-linear distribution of diffusion times, Electrochim. Acta 324 (2019) 134853, https://doi.org/10.1016/j.electacta.2019.134853.

[39] A. Hauch, K. Brodersen, M. Chen, M.B. Mogensen, Ni/YSZ electrodes structures optimized for increased electrolysis performance and durability, Solid State Ion. 293 (2016) 27–36, https://doi.org/10.1016/j.ssi.2016.06.003.

[40] A. Chrzan, S. Ovtar, P. Jasinski, M. Chen, A. Hauch, High performance LaNi1-xCoxO3-δ ($x = 0.4$ to 0.7) infiltrated oxygen electrodes for reversible solid oxide cells, J. Power Sources 353 (2017) 67–76, https://doi.org/10.1016/j.jpowsour.2017.03.148.

[41] C. Jia, M. Chen, M. Han, Performance and electrochemical analysis of solid oxide fuel cells based on LSCF-YSZ nano-electrode, Int. J. Appl. Ceram. Technol. 14 (2017) 1006–1012, https://doi.org/10.1111/ijac.12748.

[42] J.-C. Njodzefon, C.R. Graves, M.B. Mogensen, A. Weber, J. Hjelm, Kinetic studies on state of the art solid oxide cells: a comparison between Hydrogen/Steam and reformate fuels, J. Electrochem. Soc. 163 (2016) F1451–F1462, https://doi.org/10.1149/2.1201613jes.

[43] W.G. Wang, M. Mogensen, High-performance lanthanum-ferrite-based cathode for SOFC, Solid State Ion. 176 (2005) 457–462, https://doi.org/10.1016/j.ssi.2004.09.007.

[44] S. Ovtar, X. Tong, J.J. Bentzen, K.T.S. Thydén, S.B. Simonsen, M. Chen, Boosting the performance and durability of Ni/YSZ cathode for hydrogen production at high current densities: via decoration with nano-sized electrocatalysts, Nanoscale 11 (2019) 4394–4406, https://doi.org/10.1039/c8nr07678b.

[45] X. Tong, S. Ovtar, K. Brodersen, P.V. Hendriksen, M. Chen, Large-area solid oxide cells with La0.6Sr0.4CoO3-δ infiltrated oxygen electrodes for electricity generation and hydrogen production, J. Power Sources 451 (2020) 227742, https://doi.org/10.1016/j.jpowsour.2020.227742.